Relationship between the large TEC fluctuation and ionospheric echoes observed by the SuperDARN radars in the auroral zone and midlatitudes during a geomagnetic storm

Takuya Sori[1], Atsuki Shinbori[1], Yuichi Otsuka[1], Takuya Tsugawa[2], Michi Nishioka[2], William Bristow[3], J. Michael Ruohoniemi[4], Simon G. Shepherd[5], and Nozomu Nishitani[1]

[1]*Institute for Space-Earth Environmental Research, Nagoya University, Nagoya, Japan.*
[2] *National Institute of Information and Communications Technology, Koganei, Tokyo, Japan.*
[3]*Geophysical Institute, University of Alaska, Fairbanks, Alaska, United States of America.*
[4]*Virginia Tech, Blacksburg, Virginia, United States of America.*
[5]*Thayer School of Engineering, Dartmouth College, Hanover, New Hampshire, United States of America.*

Introduction

- Ionospheric irregularities

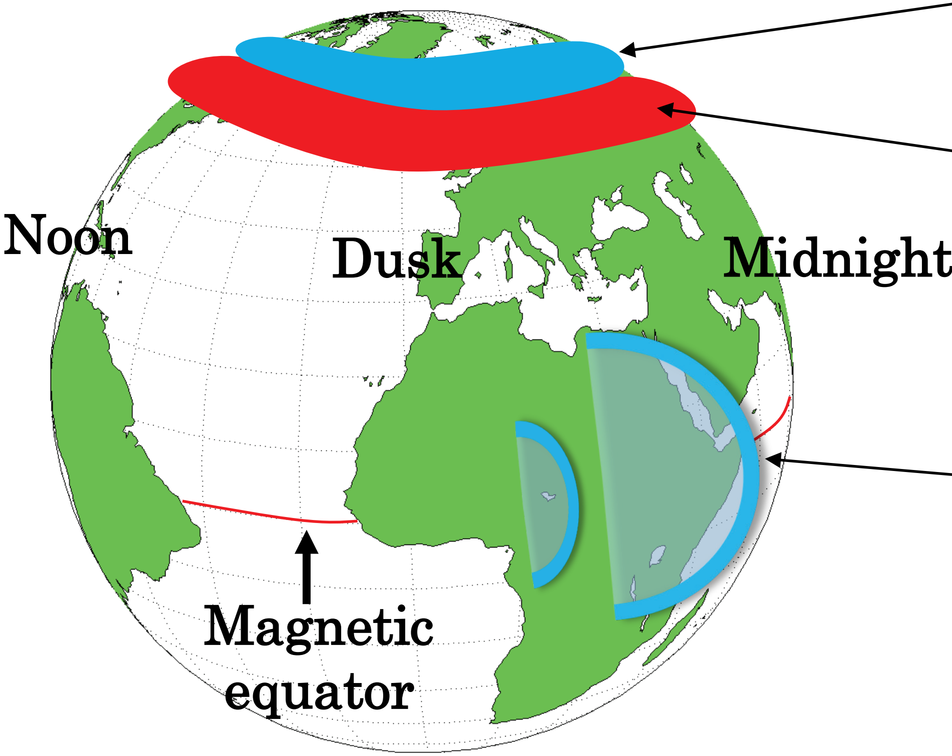

Auroral irregularities

- Cause : a particle precipitation and electric field

Sub-auroral irregularities

- Cause : a gradient drift instability

[e.g., Nishitani et al., 2019]

Low-latitude irregularities

- Cause : plasma bubbles
- Property : plasma density depletion

[Aa et al., 2018]

We found the irregularity region associated with a plasma bubble using the Global Navigation Satellite System (GNSS)-Total Electron Content (TEC) data and the midlatitude SuperDARN radar data at Fort Hays East (FHE) during a geomagnetic storm on May 27 and 28, 2017.

June 22, 2015

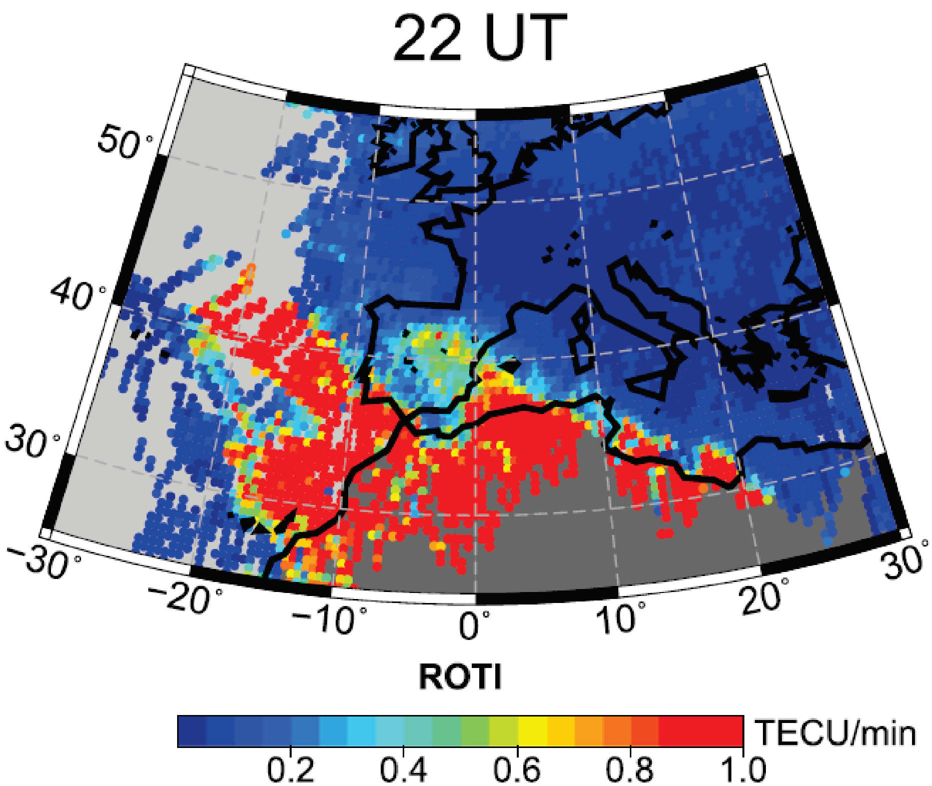

An example of storm-time mid-latitude plasma bubble in Europe as seen in the GPS-TEC variations [Cherniak and Zakharenkova, 2016]

The purpose of this study

To investigate a global distribution of ionospheric irregularities in the auroral zone and midlatitudes during the geomagnetic storm on May 27 and 28, 2017 using the GNSS-TEC data and the midlatitude SuperDARN radar data

Brief description of the Rate of TEC Index (ROTI)

Calculation method of ROTI with GNSS-TEC data

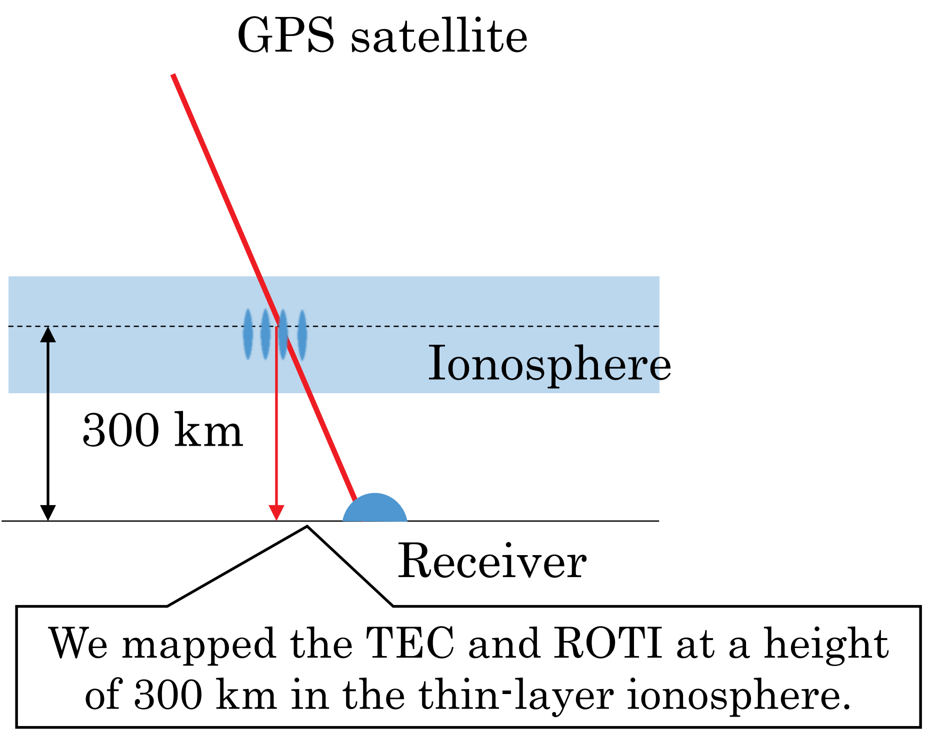

The Rate of TEC (ROT) is computed for each 30-second interval and converted to the unit of TECU/min.

ROTI is defined as the standard deviation of ROT for 5 min [Pi et al., 1997].

ROTI is a good indicator of existence of ionospheric irregularities based on the TEC data.

$$\mathrm{ROT} = \frac{\mathrm{T}\,(\mathrm{t}_0+0.5)-\mathrm{T}\,(\mathrm{t}_0)}{0.5}\ [TECU/min]$$

T (t) [TECU] : TEC at time t
([TECU] = $[10^{16}/m^2]$)

$$\mathrm{ROTI} = \sqrt{\langle \mathrm{ROT}^2\rangle - \langle \mathrm{ROT}\rangle^2}\ [TECU/min]$$

Comparison between SuperDARN radar and ROTI data

	Coverage	Scale of irregularity	Temporal resolution
SuperDARN radar data	field of view	decameter-scale	1 min
ROTI data	global	3-30 km	5 min

In this study, we use both the SuperDARN radar data and GNSS-ROTI data to capture the ionospheric irregularities with different scales.

Data sources

- Global GNSS-TEC data with high temporal and spatial resolutions are provided by National Institute of Information and Communications Technology (NICT).

- The SYM-H index is provided by WDC, Kyoto University.

- The solar wind and interplanetary magnetic field data are provided by Coordinated Data Analysis Web (CDAWeb), NASA (https://cdaweb.sci.gsfc.nasa.gov/ index/.html).

- Midlatitude SuperDARN radar data at Adak Island East (ADE), Adak Island West (ADW), Blackstone (BKS), Christmas Valley East (CVE), Christmas Valley West (CVW), Fort Hays East (FHE), Fort Hays West (FHW), Hokkaido West (HKW), and Hokkaido East (HOK) are provided by ERG Science Center, Nagoya University.

An overview of geomagnetic storm on May 27 and 28, 2017

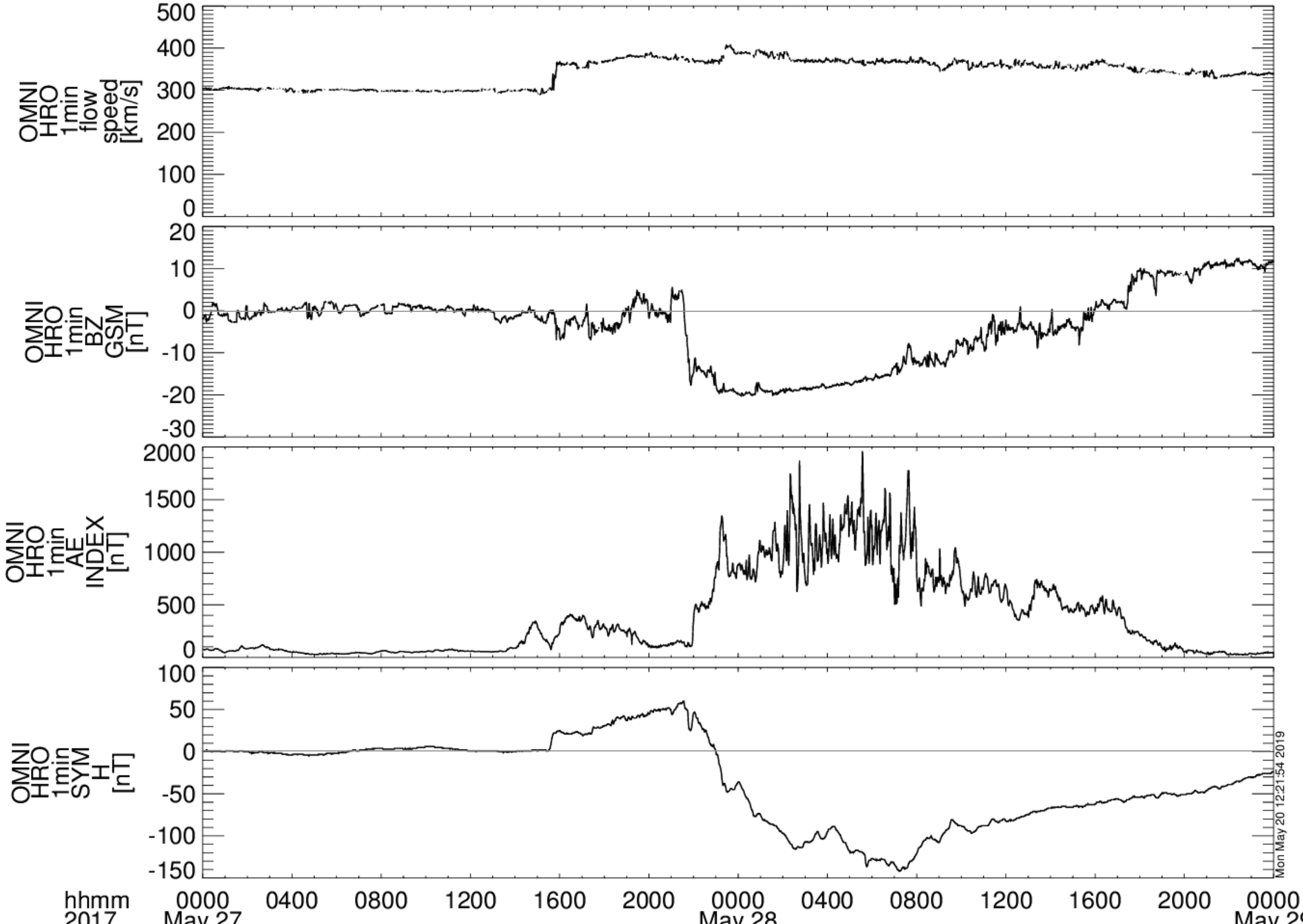

- The north–south (Bz) component of the IMF shows a minimum value of -20 nT on May 27 and 28.
- Corresponding to the period, the SYM-H index shows a significant decrease with a minimum value of -150 nT at 07:00 UT on May 28.

Polar map of ROTI in the Northern Hemisphere

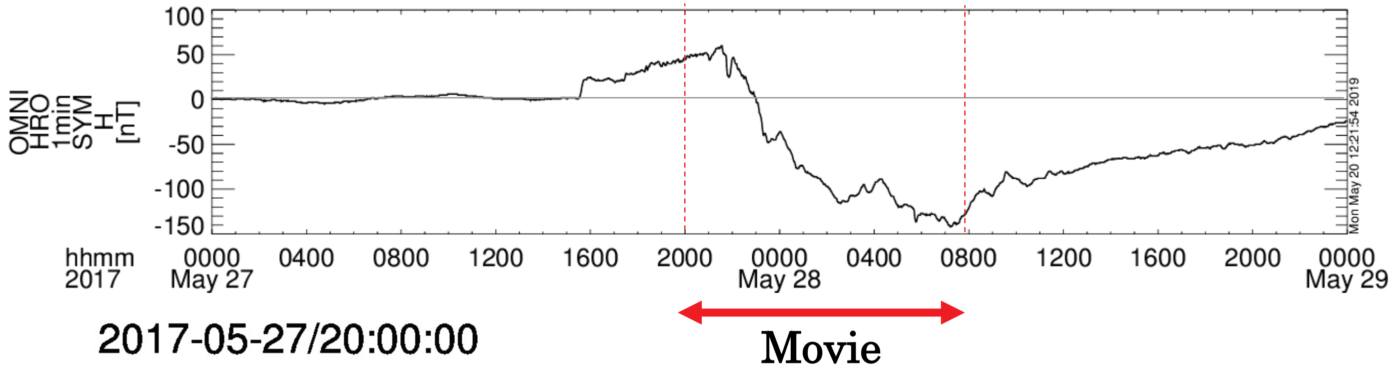

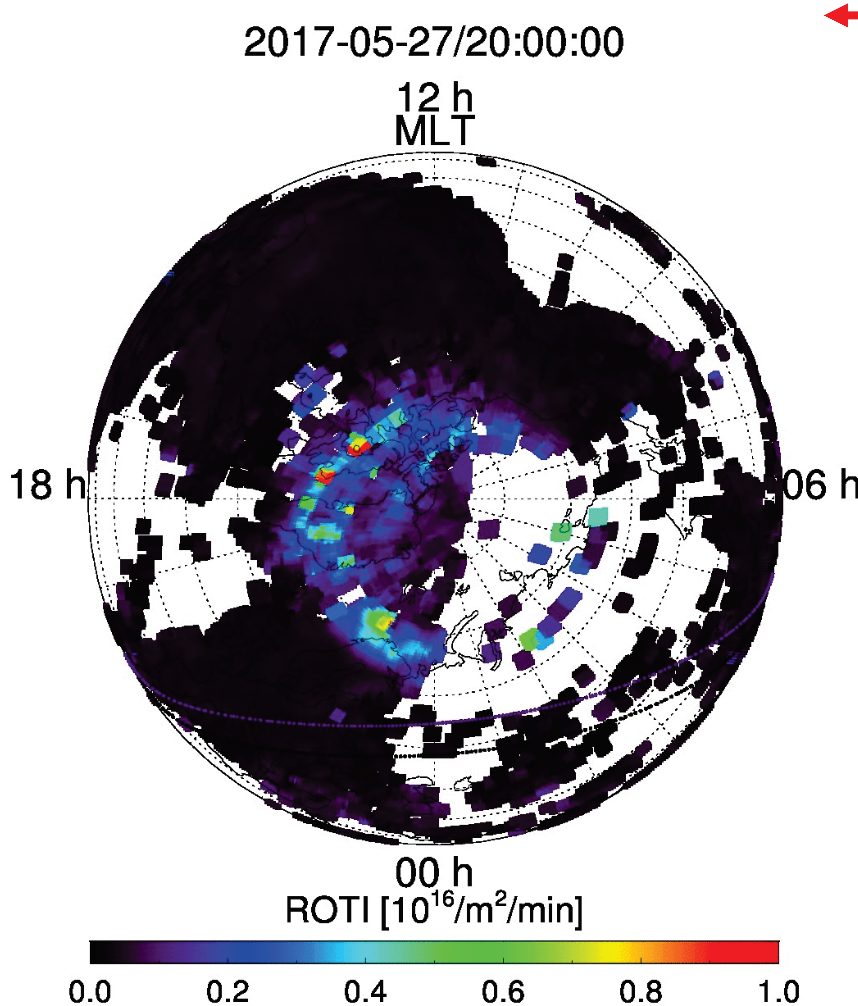

The enhanced ROTI region associated with the auroral oval and the equatorward wall of midlatitude trough moves equatorward during the main phase of the geomagnetic storm.

Another enhanced ROTI region appears at low latitude in North America at 01:00 UT on May 28, and moves to the midlatitude of 50°N in geomagnetic latitude.

↑

Plasma bubble

Polar map of ROTI and backscatter power

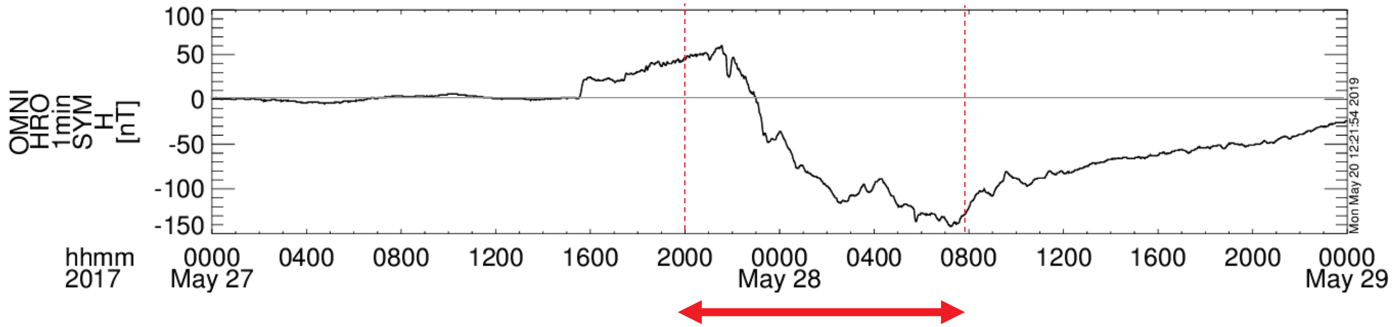

Movie

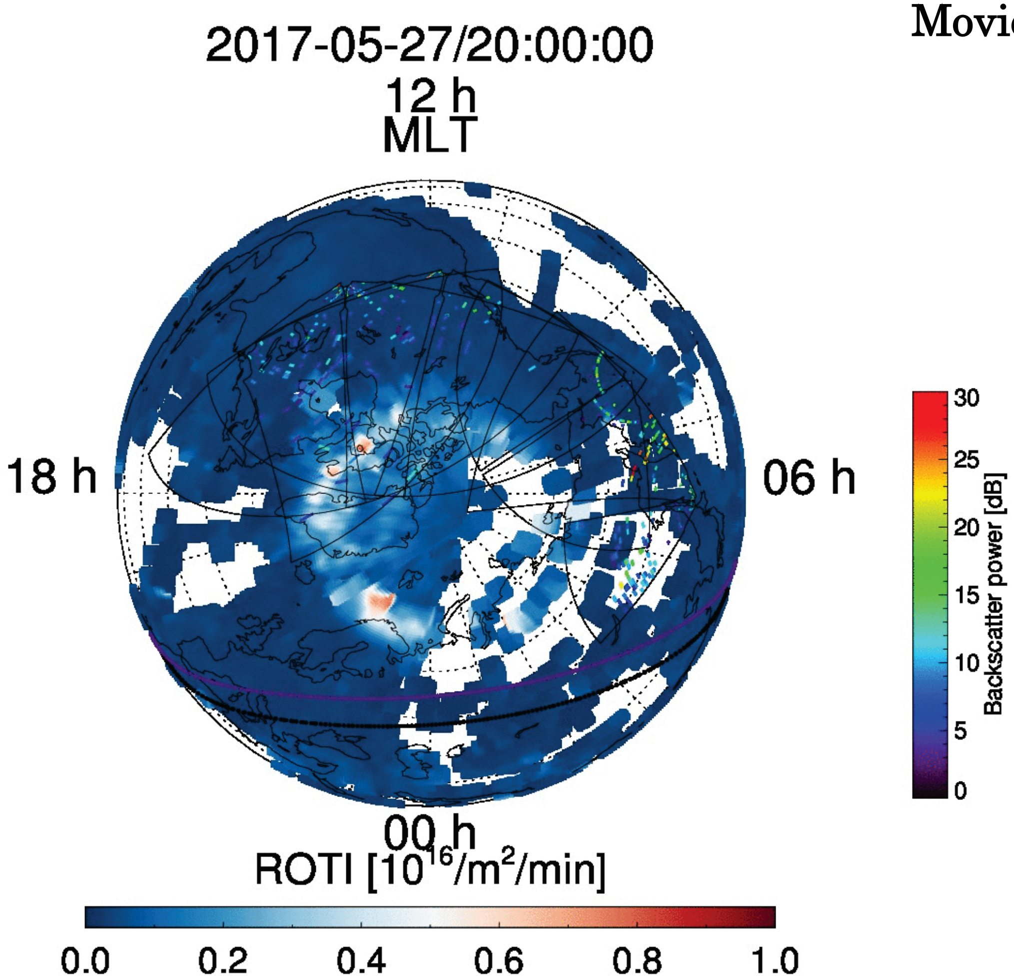

The ionospheric field-aligned irregularity (FAI) echoes associated with the auroral oval and the equatorward wall of midlatitude trough appear during the main phase of the geomagnetic storm until 04:00 UT on May 28.

Most of the ionospheric FAI echoes coincide with the enhanced ROTI region and move equatorward.

Polar map of ROTI and backscatter power

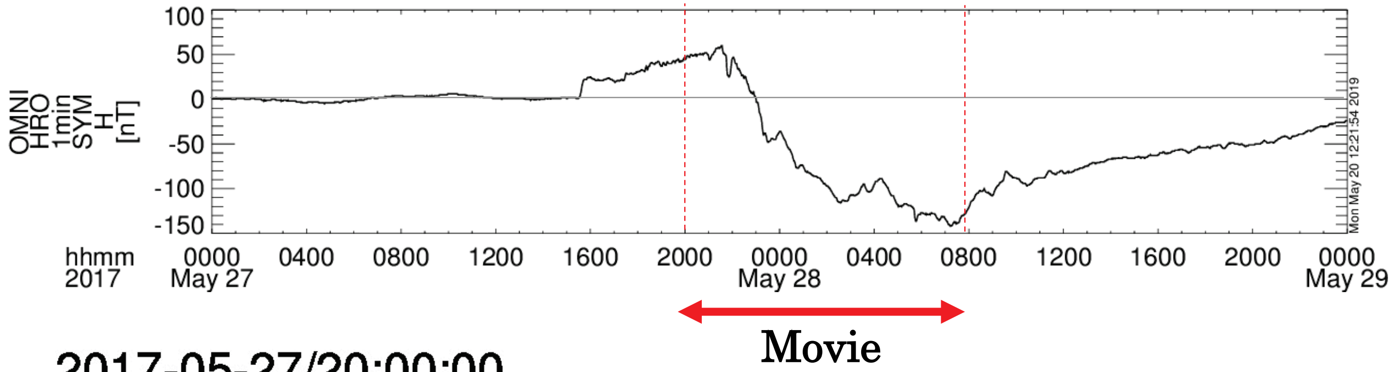

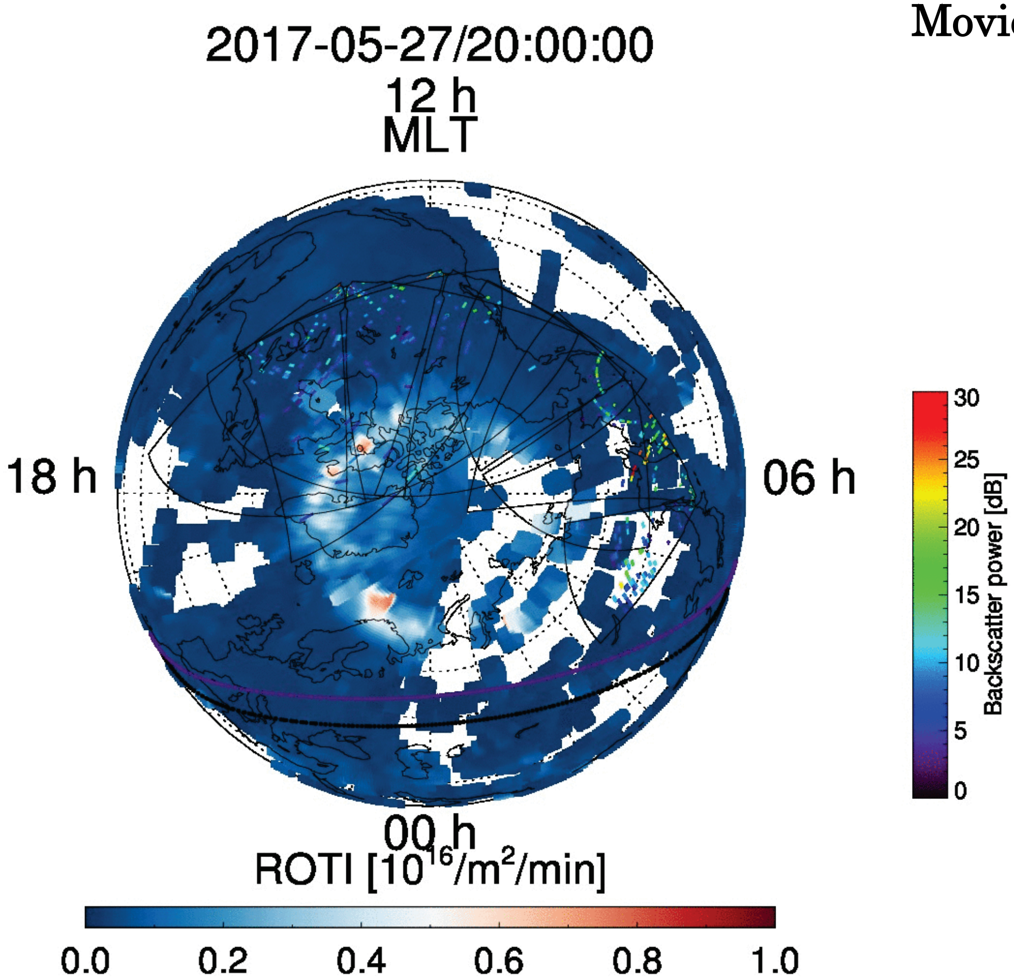

After 04:00 UT on May 28, the ionospheric FAI echoes almost disappear in spite of existence of the enhanced ROTI region.

Range gate-time plots of ROTI and CVE radar beam-0 backscatter power

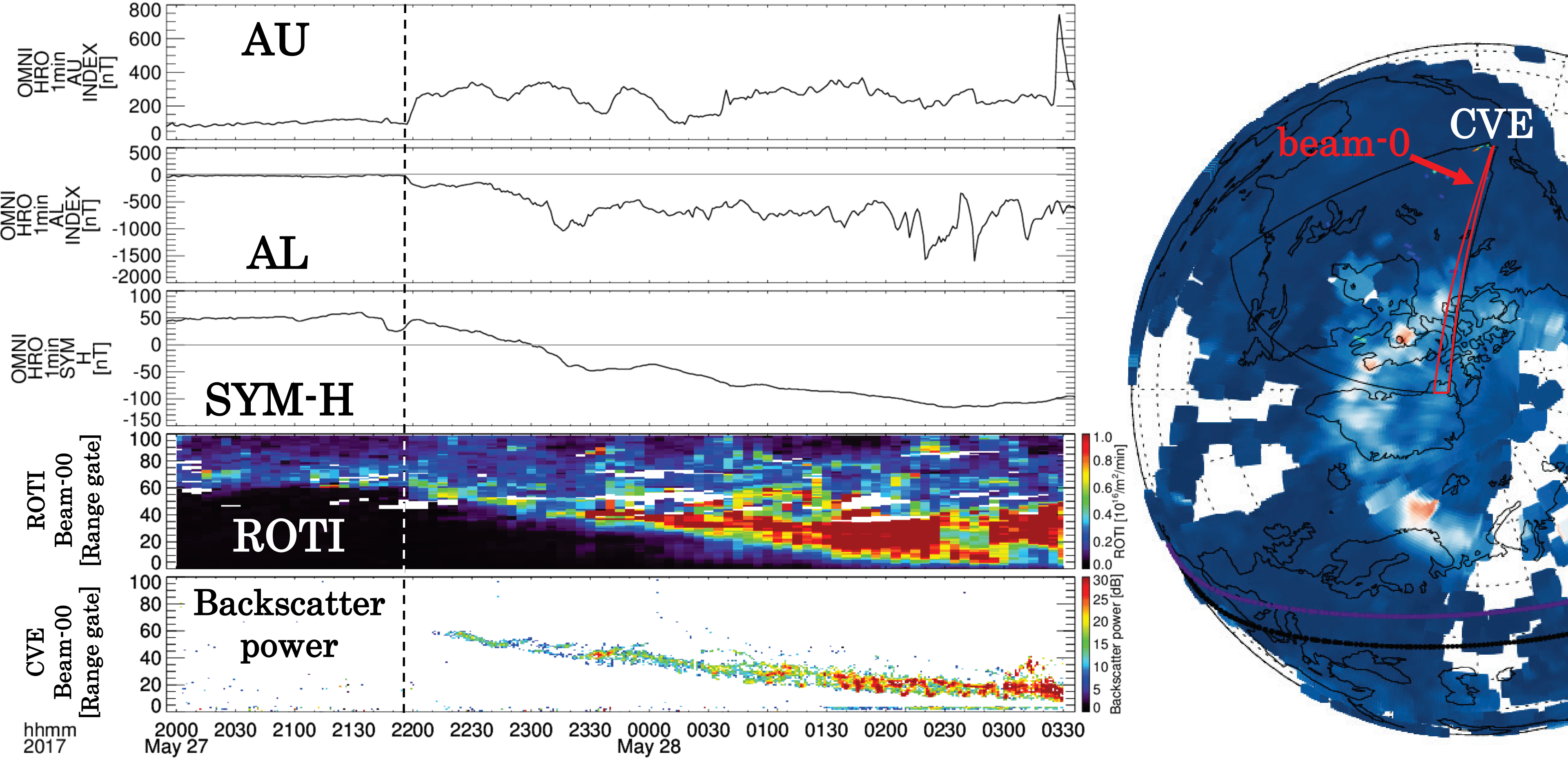

・After 22:00 UT on May 27, the enhanced ROTI region moves equatorward with the development of the geomagnetic storm.

・FAI echoes at the CVE radar beam-0 tend to appear along the enhanced ROTI region.

Range gate-time plots of ROTI and CVE radar beam-0 backscatter power

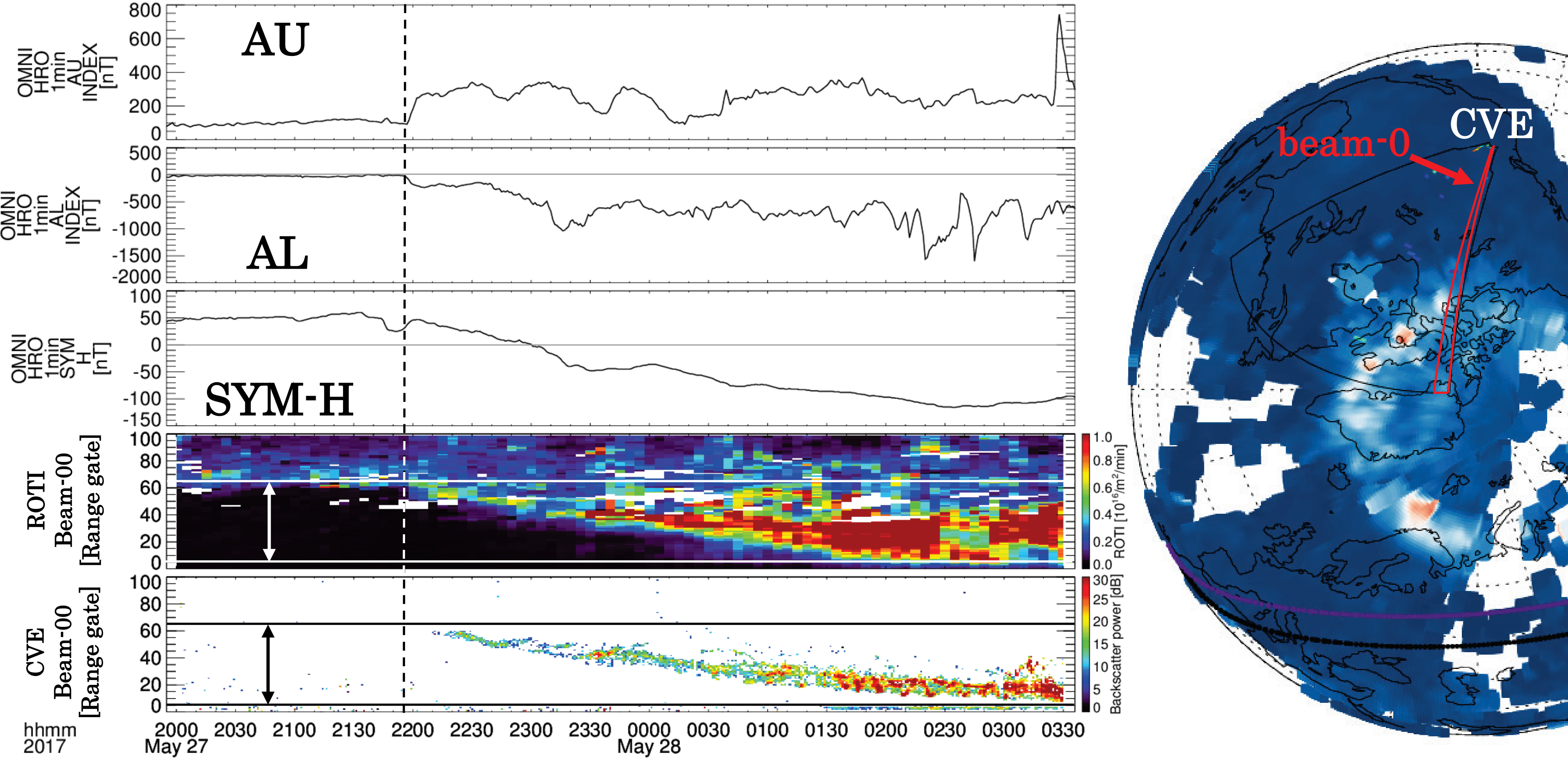

We compare the values of ROTI and backscatter power along beam-0 at CVE radar in the F-region of the ionosphere between 5 and 65 range gate.

Time interval is from 20:00 UT on May 27 to 03:30 UT on May 28.

ROTI-backscatter power plot along CVE radar beam-0

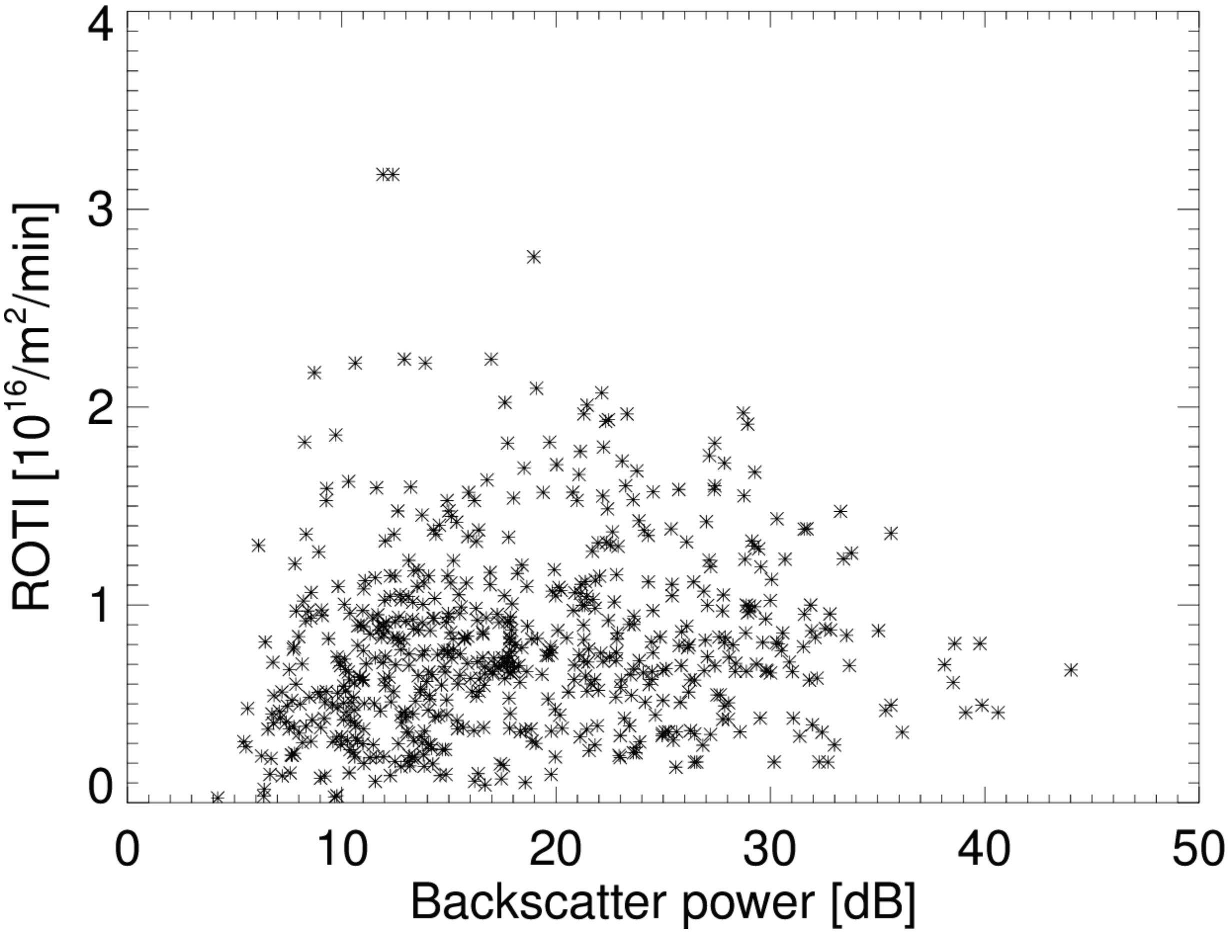

- The correlation coefficient is 0.081.

- The ionospheric FAI echoes observed by the CVE radar along the beam-0 direction tend to distribute in the enhanced ROTI region, but there is no correlation between the values of ROTI and backscatter power.

Plasma bubble

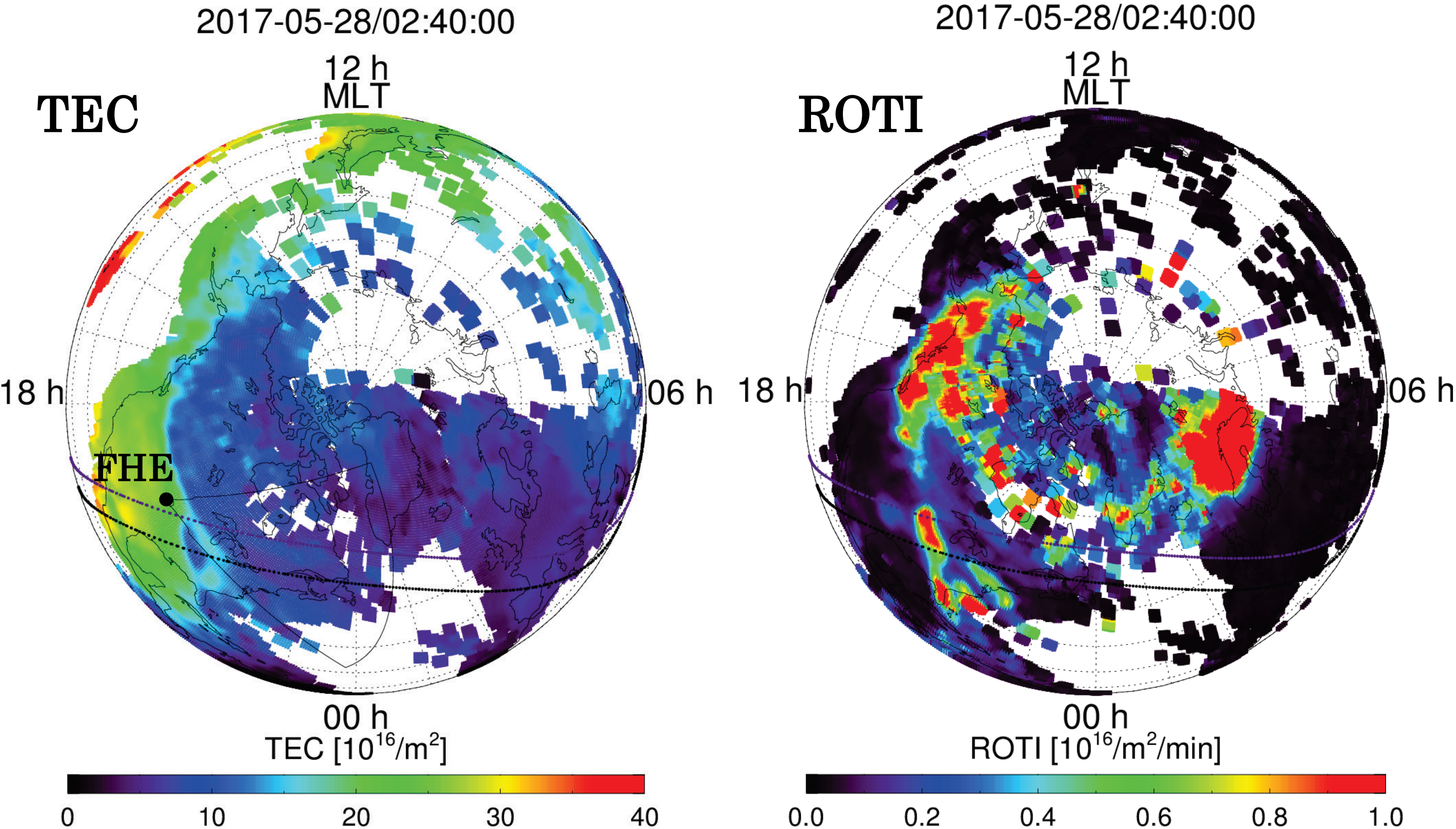

- The midlatitude plasma bubble with the TEC depletion and the enhanced ROTI region enters the field of view of the FHE radar around 02:30 UT.

Plasma bubble

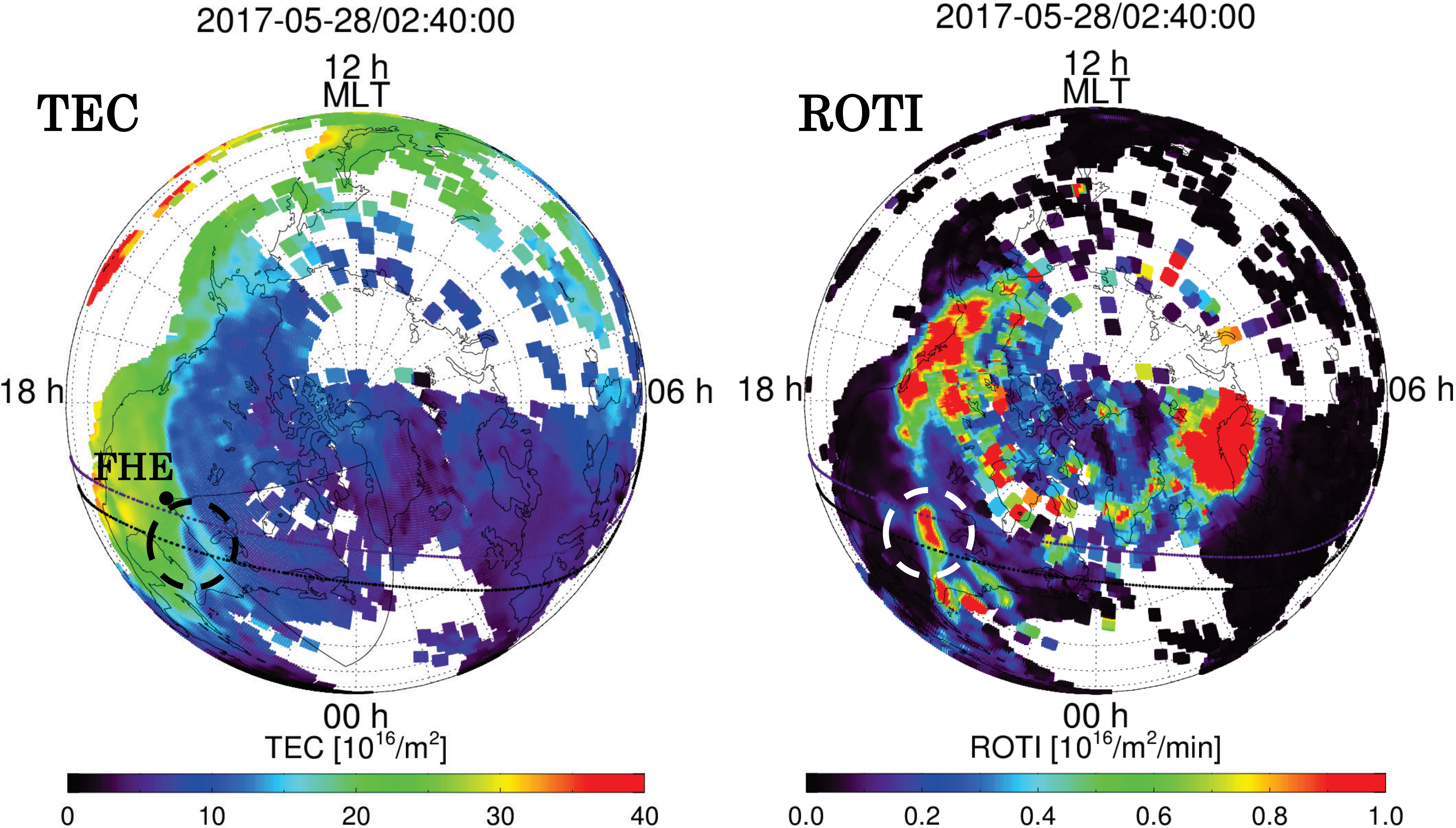

・The midlatitude plasma bubble with the TEC depletion and the enhanced ROTI region enters the field of view of the FHE radar around 02:30 UT.

Plasma bubble

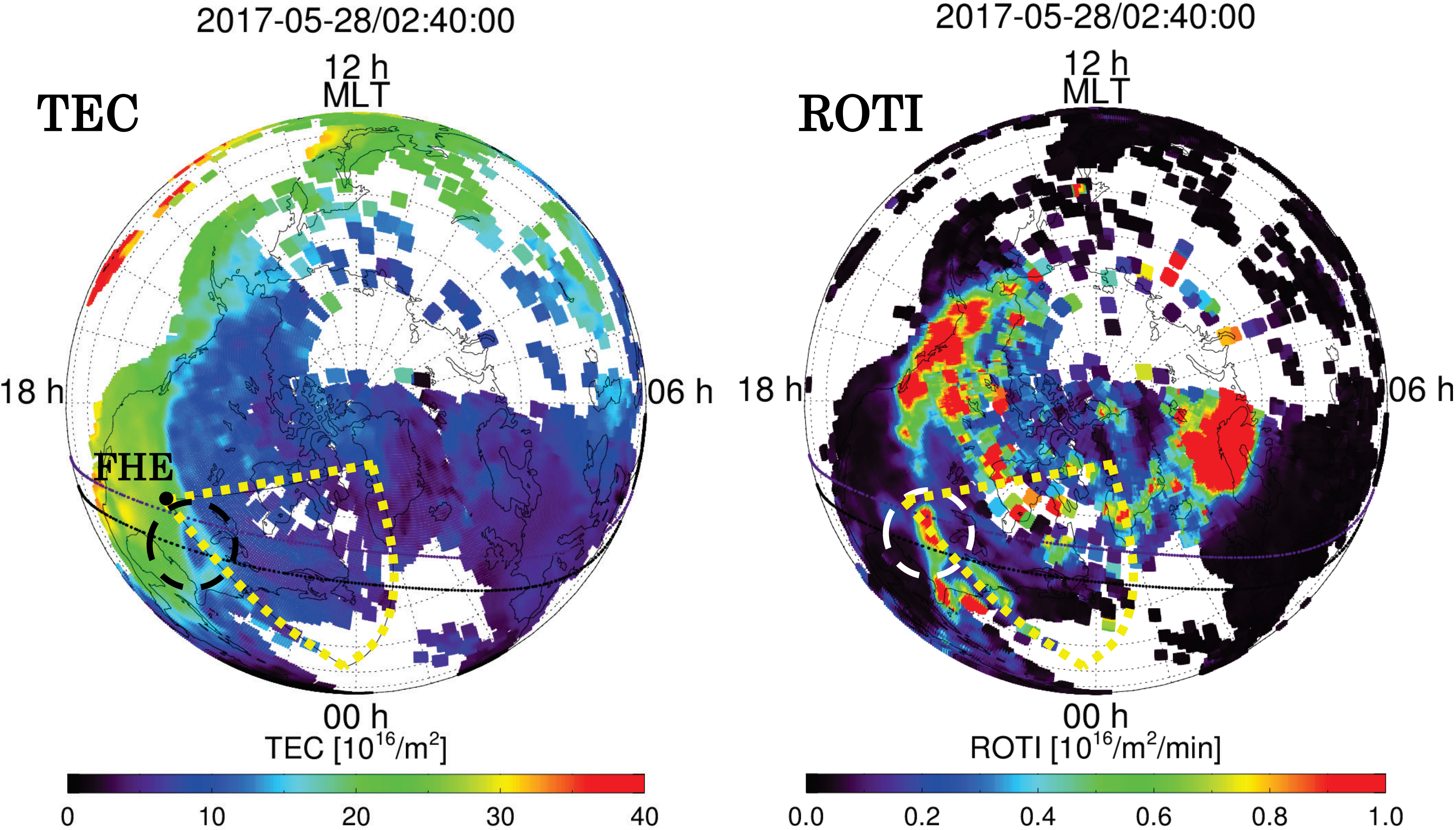

・The midlatitude plasma bubble with the TEC depletion and the enhanced ROTI region enters the field of view of the FHE radar around 02:30 UT.

Range gate-time plot along the FHE radar beam-20 direction

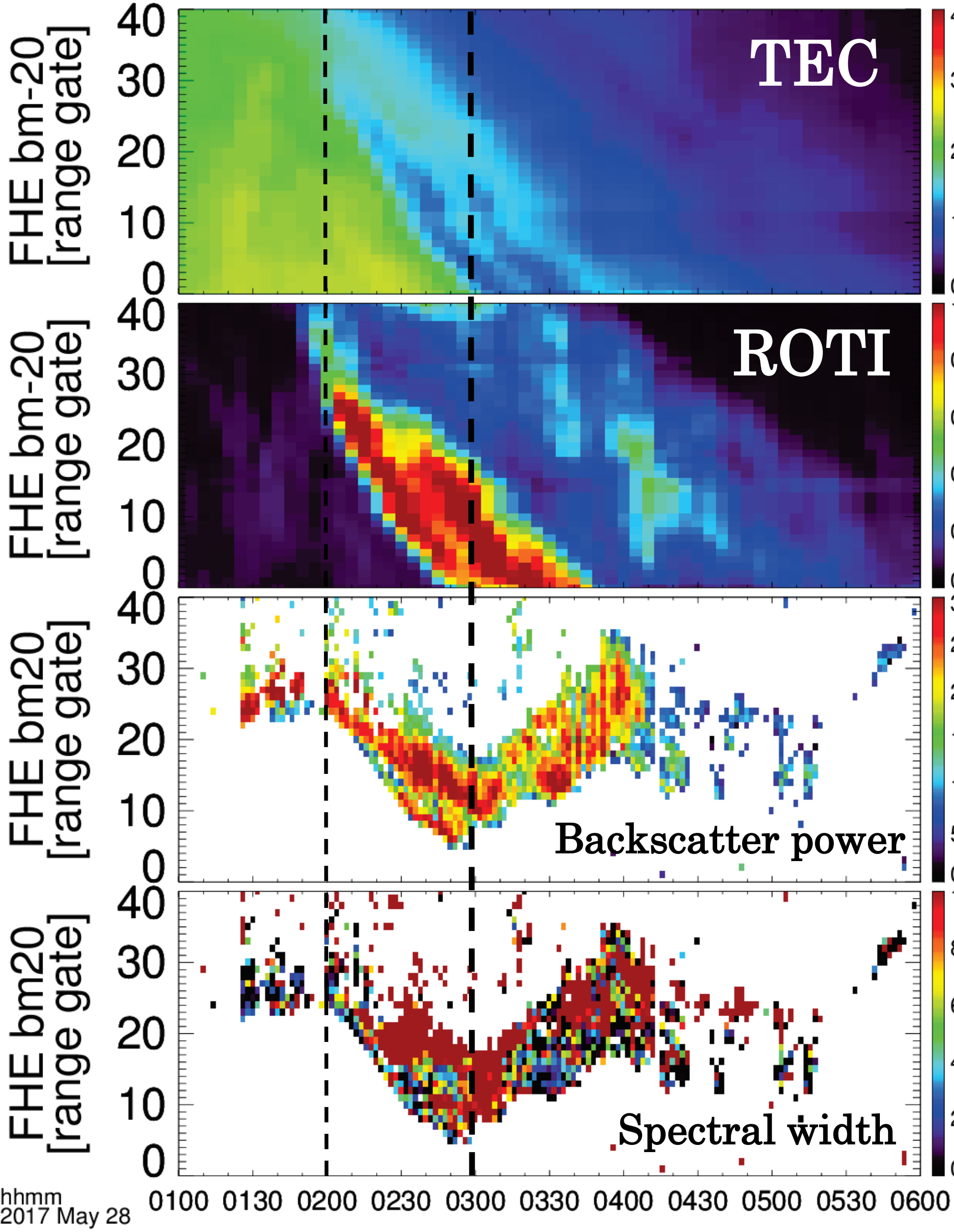

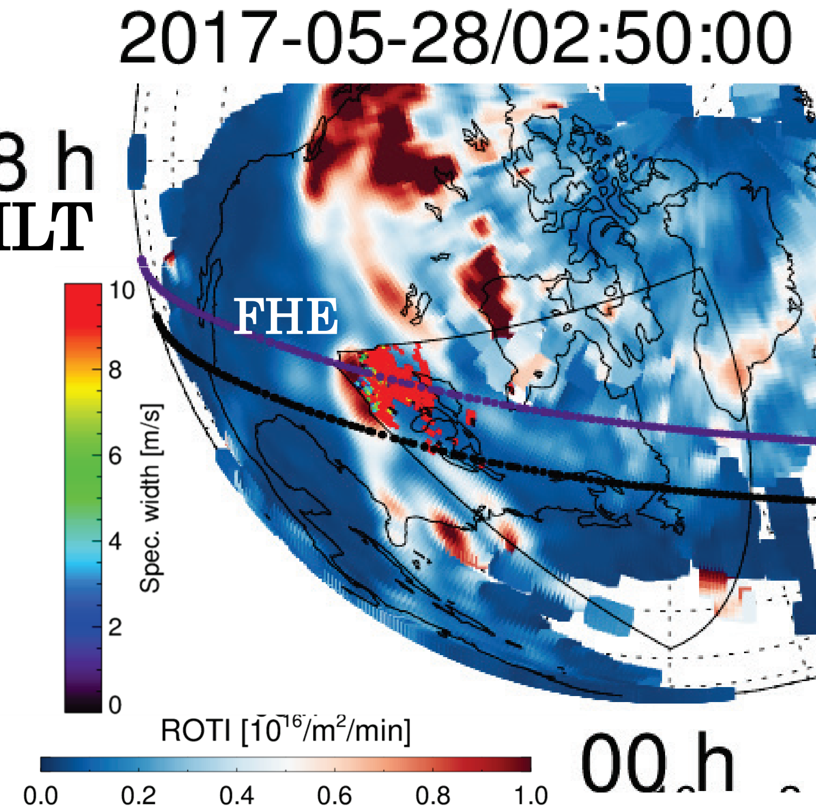

- A narrow spectral width is observed by the FHE radar beam-20 between 02:00 and 03:00 UT when the enhanced ROTI region enters the field of view of FHE radar.

Range gate-time plot along the FHE radar beam-20 direction

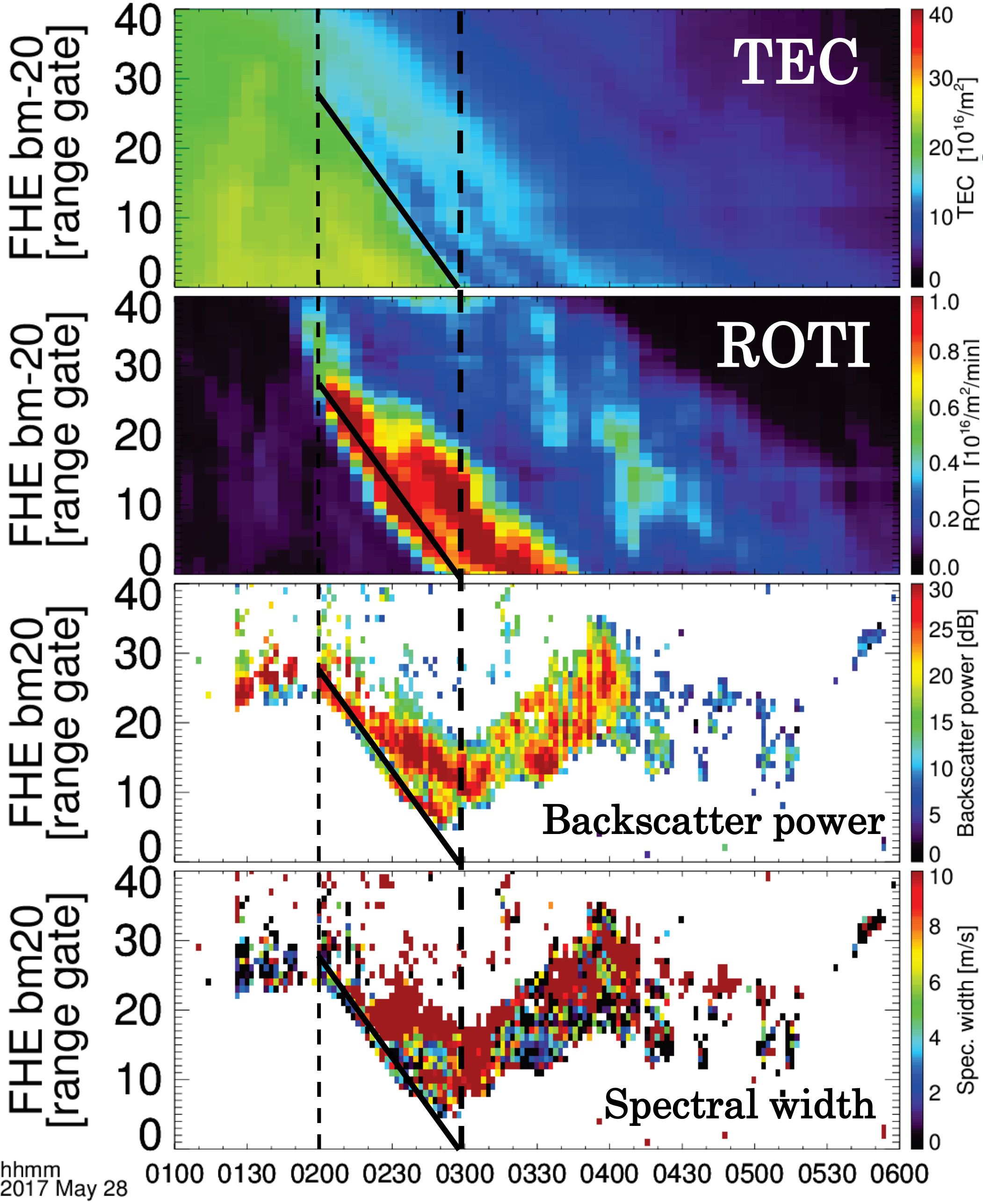

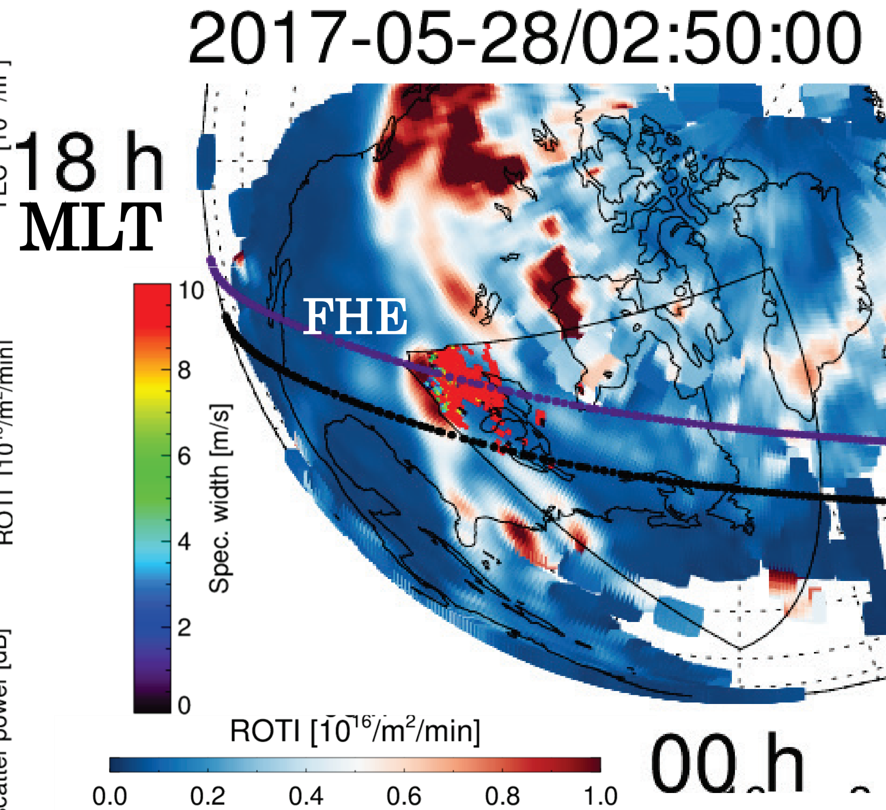

- A narrow spectral width is observed by the FHE radar beam-20 between 02:00 and 03:00 UT when the enhanced ROTI region enters the field of view of FHE radar.

Discussion

・The ionospheric FAI echoes associated with the auroral oval and the equatorward wall of midlatitude trough appear during the main phase of the geomagnetic storm, corresponding to the enhanced ROTI region.

・However, after 04:00 UT on May 28, the ionospheric FAI echoes almost disappear in spite of existence of the enhanced ROTI region.

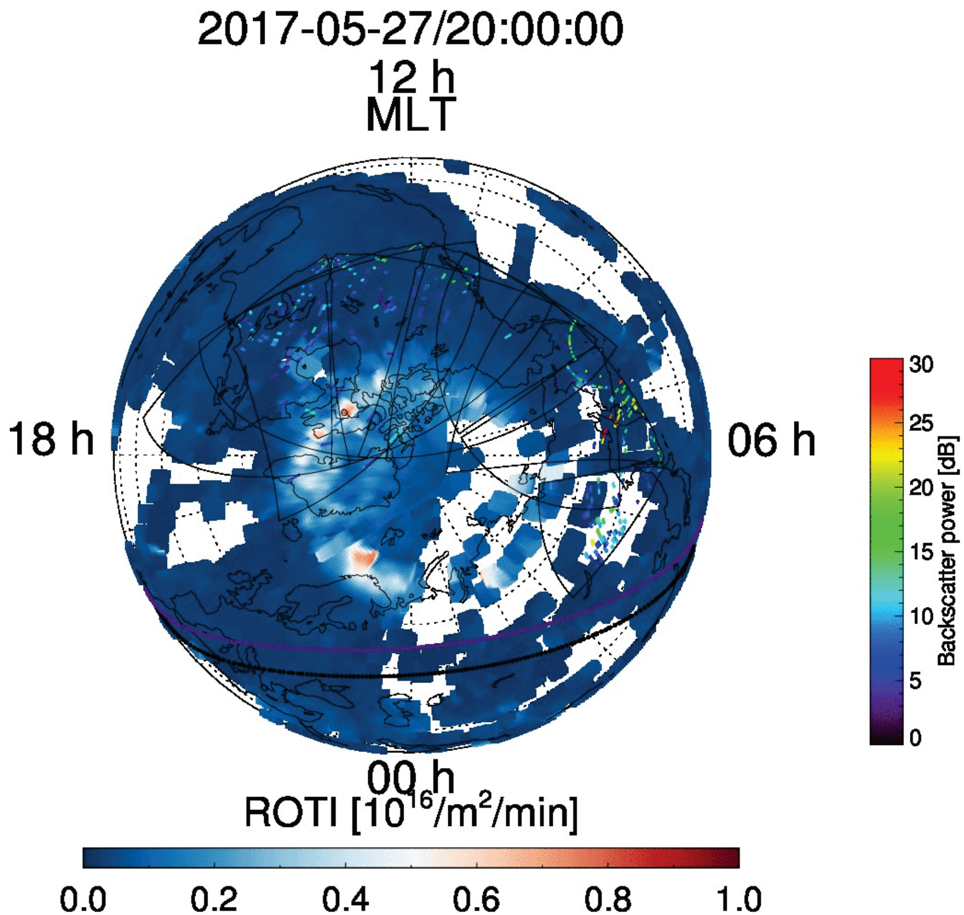

・The ionospheric irregularity with decameter-scale disappears after 04:00 UT on May 28.

or

・The ionospheric FAI echoes are absorbed due to the enhanced D-region associated with high energy electron precipitation after 04:00 UT on May 28.

We need further studies about the increasing electron density in D-region during this interval in order to verify this hypothesis.

Discussion

・The ionospheric FAI echoes observed by the FHE radar beam-20 associated with the midlatitude plasma bubble have a narrow spectral width.

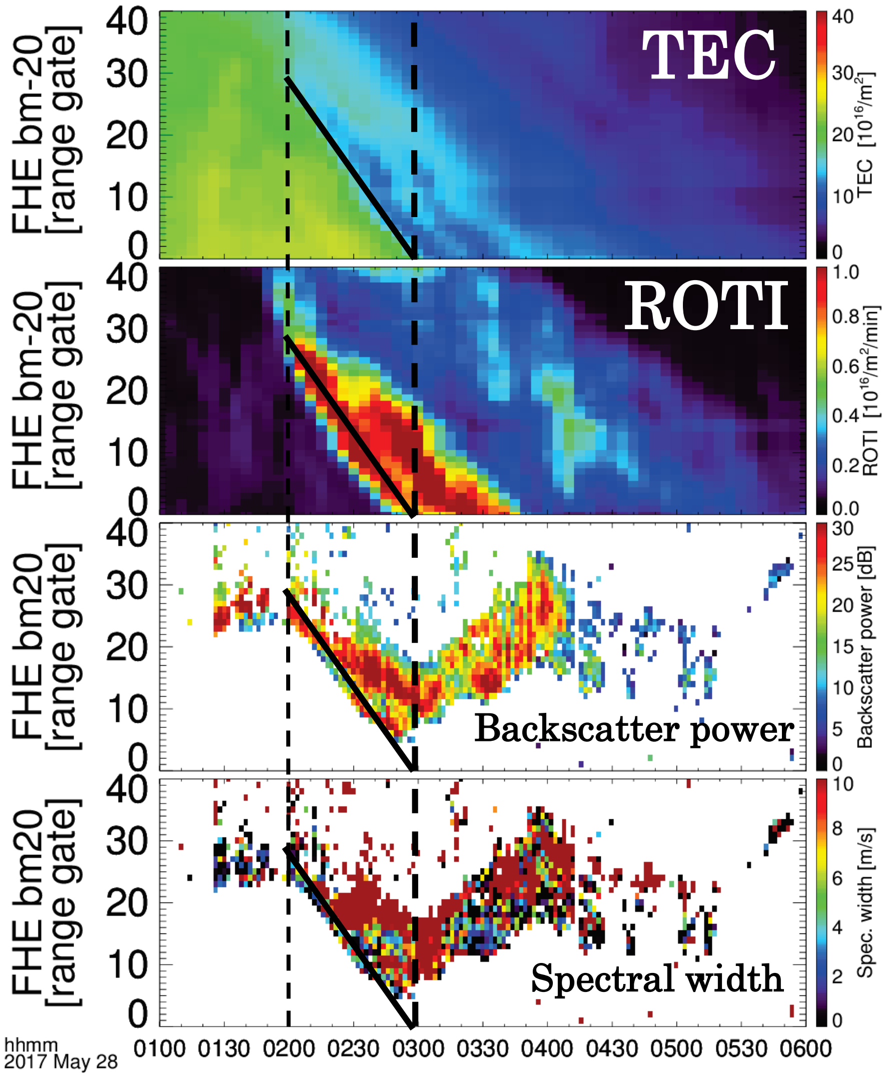

・Narrow spectral width indicates that there is no turbulence inside the midlatitude plasma bubble.

→The enhanced ROTI region can expand up to 50°N in geomagnetic latitude, keeping a large spatial structure.

The midlatitude plasma bubble can be observed by midlatitude SuperDARN radars during large geomagnetic storms.

Conclusions

We analyze the global distributions of ROTI and the ionospheric FAI echoes during a geomagnetic storm on May 27 and 28, 2017.

1. The ionospheric FAI echoes associated with the auroral oval and the equatorward wall of midlatitude trough appear during the main phase of the geomagnetic storm, corresponding to the enhanced ROTI region.
2. There is no correlation (0.081) between the values of ROTI and backscatter power.

1. The midlatitude plasma bubble appears at low latitude in North America at 01:00 UT on May 28, and moves to the midlatitude of 50°N in geomagnetic latitude.
2. A narrow spectral width is observed by the FHE radar beam-20 between 02:00 and 03:00 UT when the enhanced ROTI region enters the field of view of the FHE radar.

The midlatitude plasma bubble can be observed by midlatitude SuperDARN radars during large geomagnetic storms.

Polar map of SuperDARN echoes in Northern Hemisphere

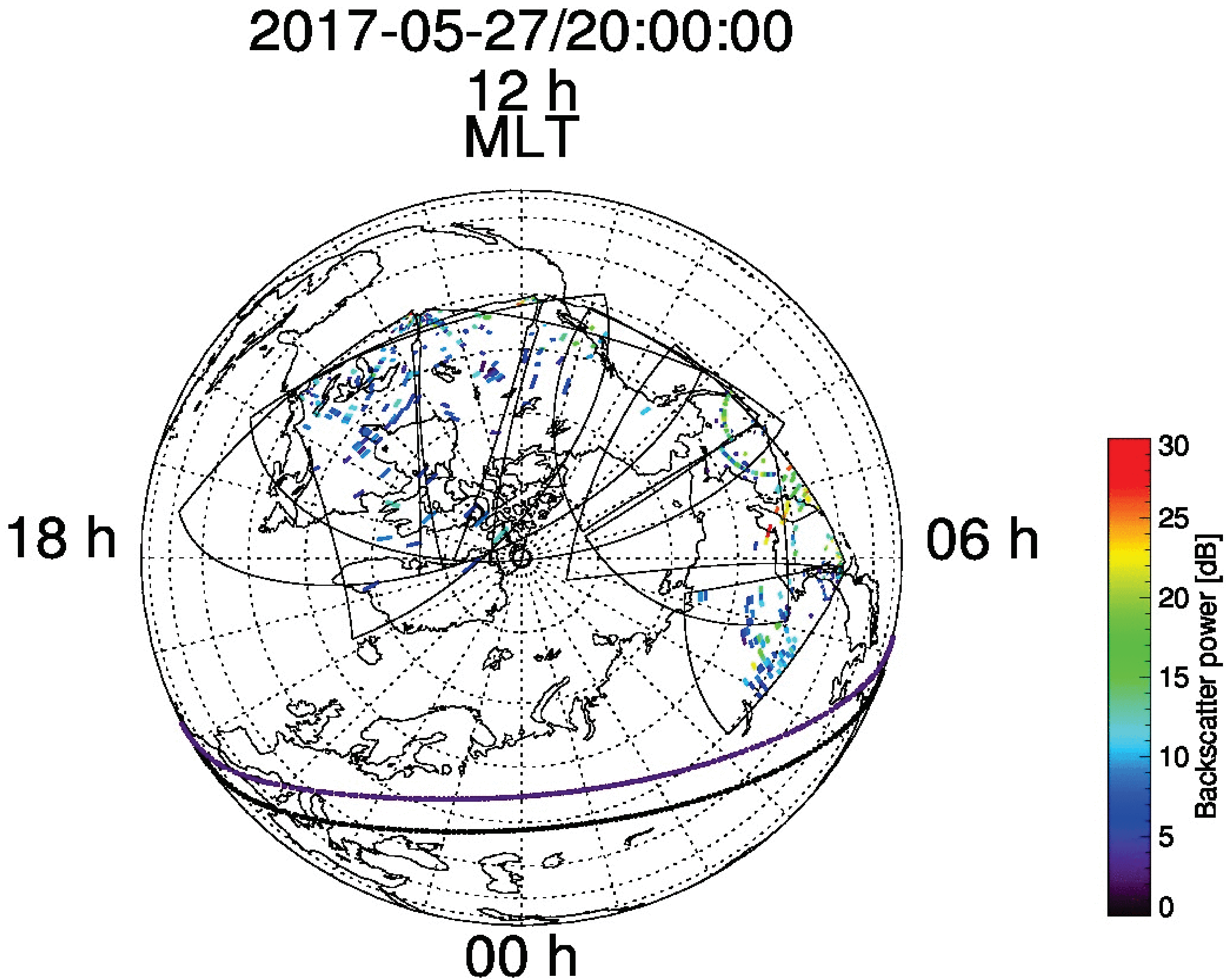

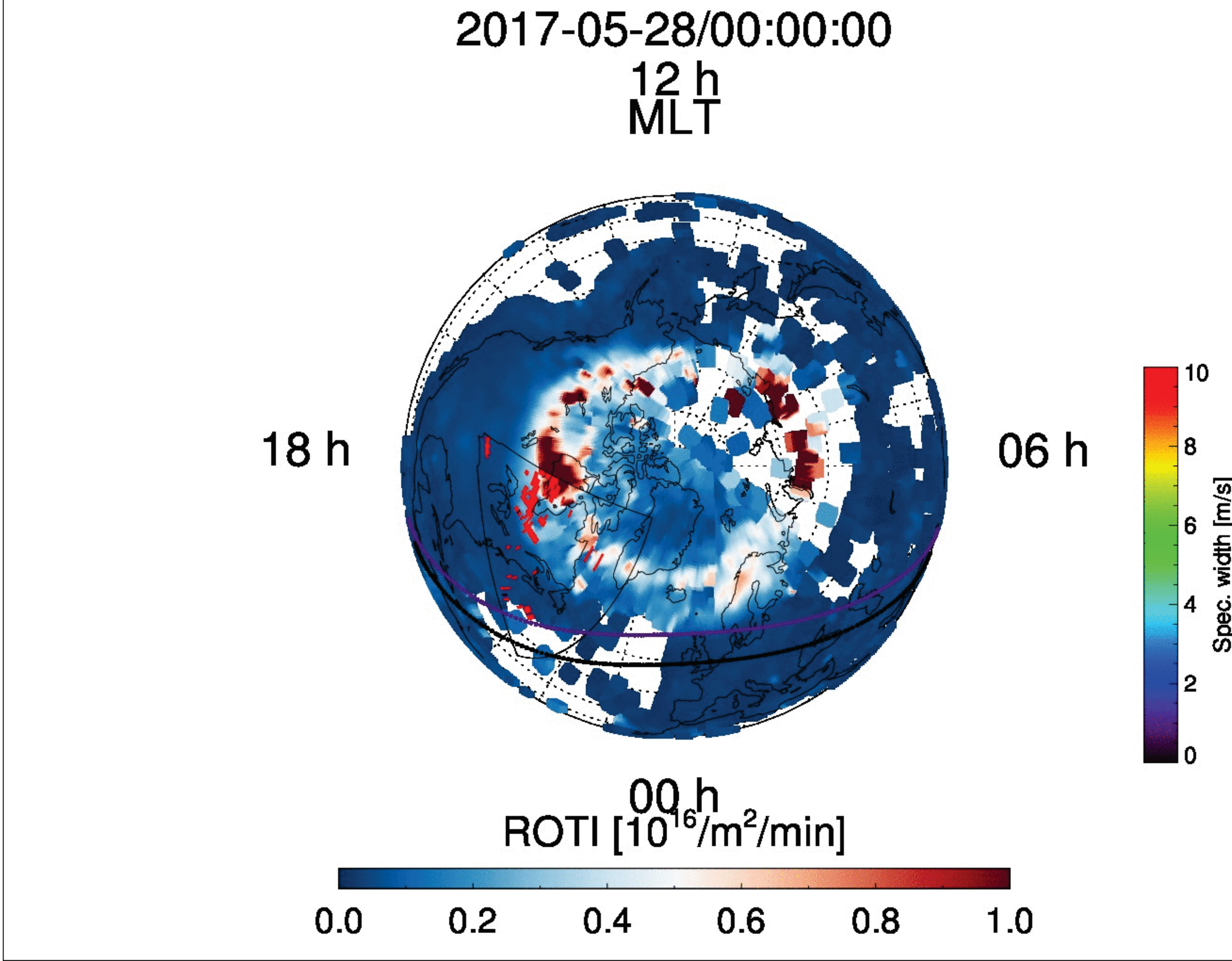
2017-05-28/00:00:00
12 h
MLT
18 h
06 h
00 h
ROTI [10^16/m^2/min]
0.0
0.2
0.4
0.6
0.8
1.0
Spec. width [m/s]
0
2
4
6
8
10

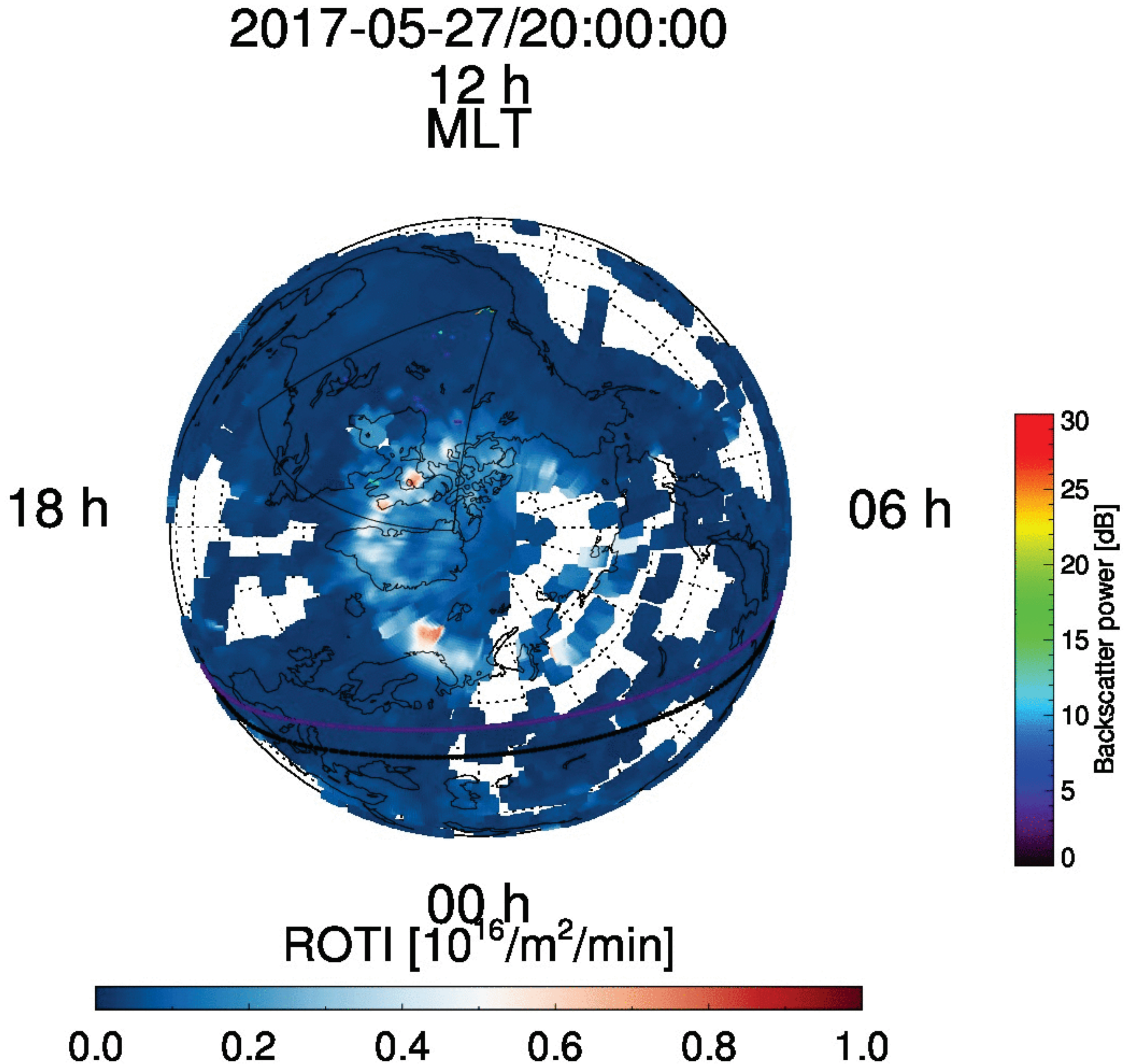
2017-05-27/20:00:00
12 h
MLT
18 h
06 h
00 h
Backscatter power [dB]
30
25
20
15
10
5
0
ROTI [10^16/m^2/min]
0.0
0.2
0.4
0.6
0.8
1.0

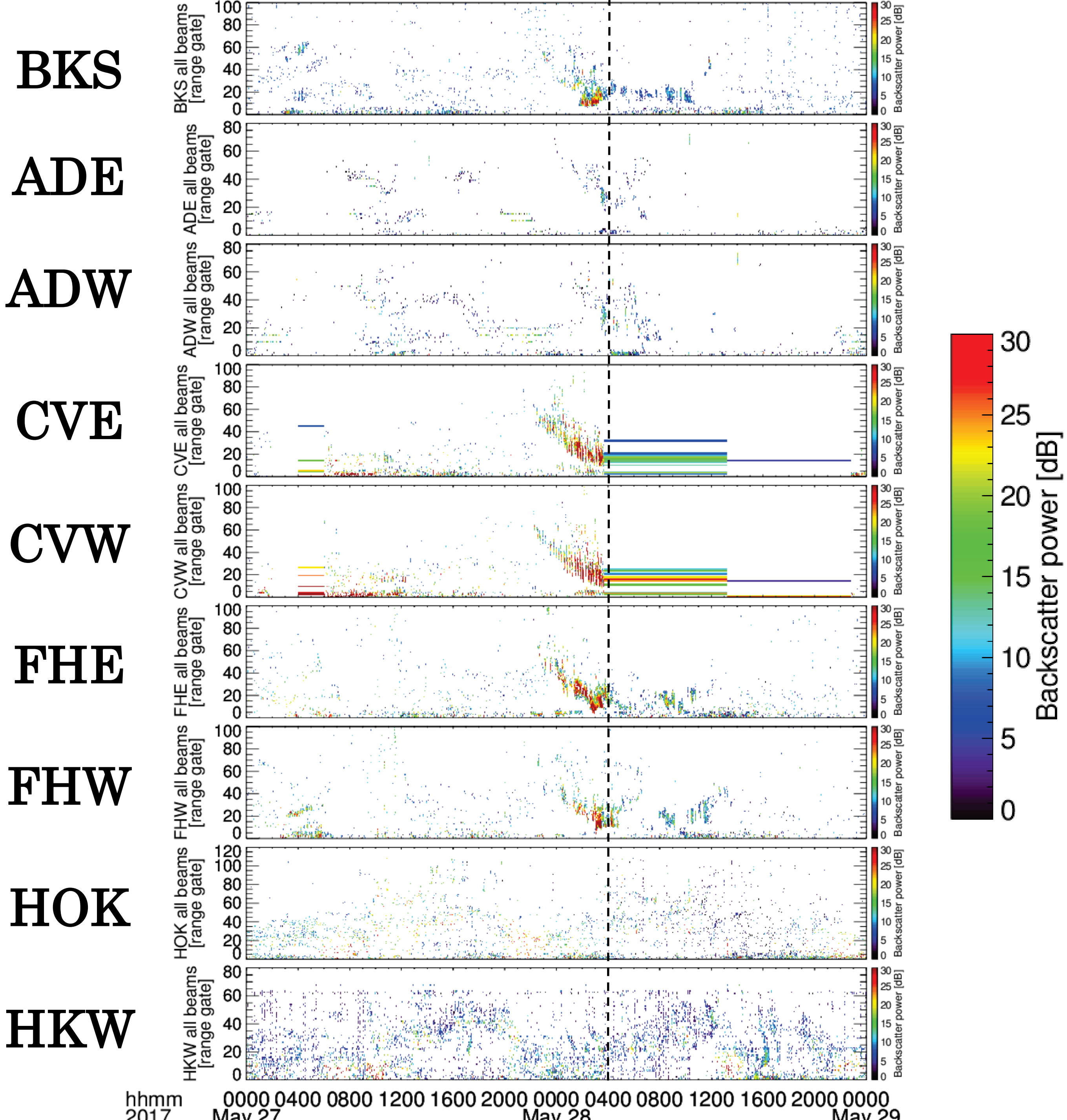

BKS
ADE
ADW
CVE
CVW
FHE
FHW
HOK
HKW
BKS all beams [range gate]
ADE all beams [range gate]
ADW all beams [range gate]
CVE all beams [range gate]
CVW all beams [range gate]
FHE all beams [range gate]
FHW all beams [range gate]
HOK all beams [range gate]
HKW all beams [range gate]
Backscatter power [dB]
hhmm 2017
0000 0400 0800 1200 1600 2000 0000 0400 0800 1200 1600 2000 0000
May 27
May 28
May 29

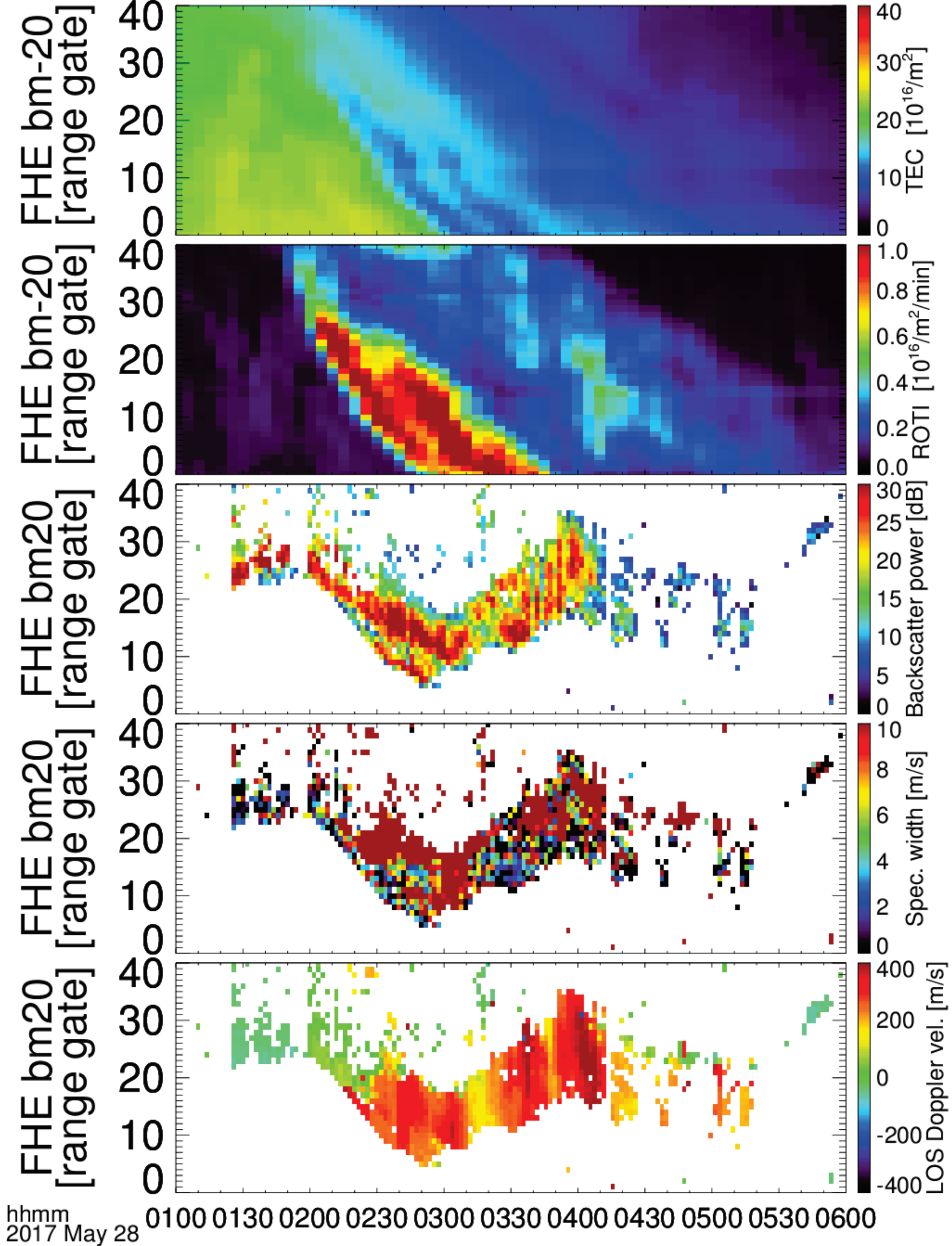

FHE bm-20 [range gate]
TEC [10^16/m^2]
ROTI [10^16/m^2/min]
FHE bm20 [range gate]
Backscatter power [dB]
Spec. width [m/s]
LOS Doppler vel. [m/s]
hhmm
2017 May 28
0100 0130 0200 0230 0300 0330 0400 0430 0500 0530 0600

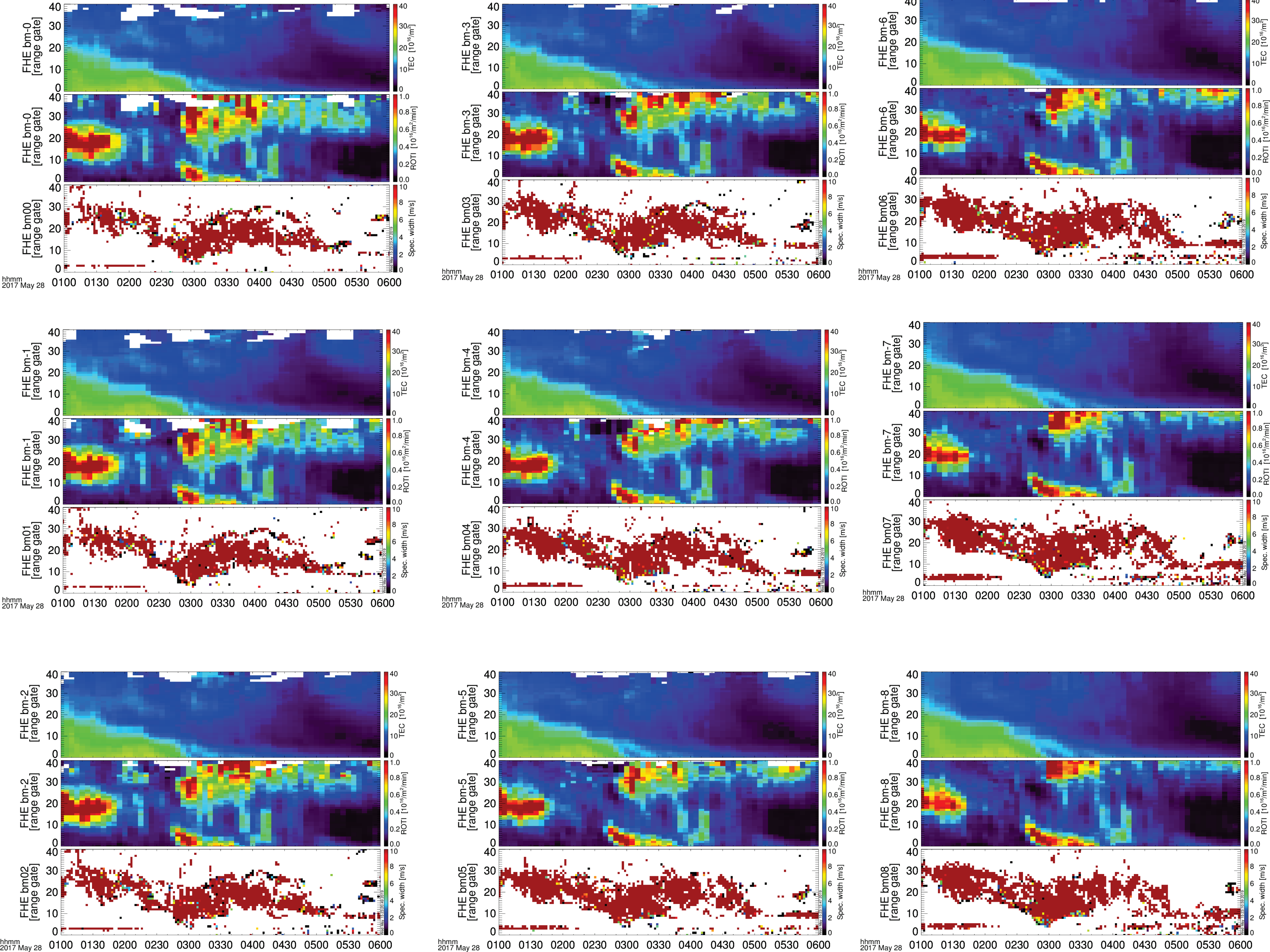
FHE bm-0 [range gate]
TEC [10^16/m^2]
ROTI [10^16/m^2/min]
FHE bm00 [range gate]
Spec. width [m/s]
hhmm
2017 May 28
0100 0130 0200 0230 0300 0330 0400 0430 0500 0530 0600
FHE bm-1 [range gate]
FHE bm01 [range gate]
FHE bm-2 [range gate]
FHE bm02 [range gate]
FHE bm-3 [range gate]
FHE bm03 [range gate]
FHE bm-4 [range gate]
FHE bm04 [range gate]
FHE bm-5 [range gate]
FHE bm05 [range gate]
FHE bm-6 [range gate]
FHE bm06 [range gate]
FHE bm-7 [range gate]
FHE bm07 [range gate]
FHE bm-8 [range gate]
FHE bm08 [range gate]

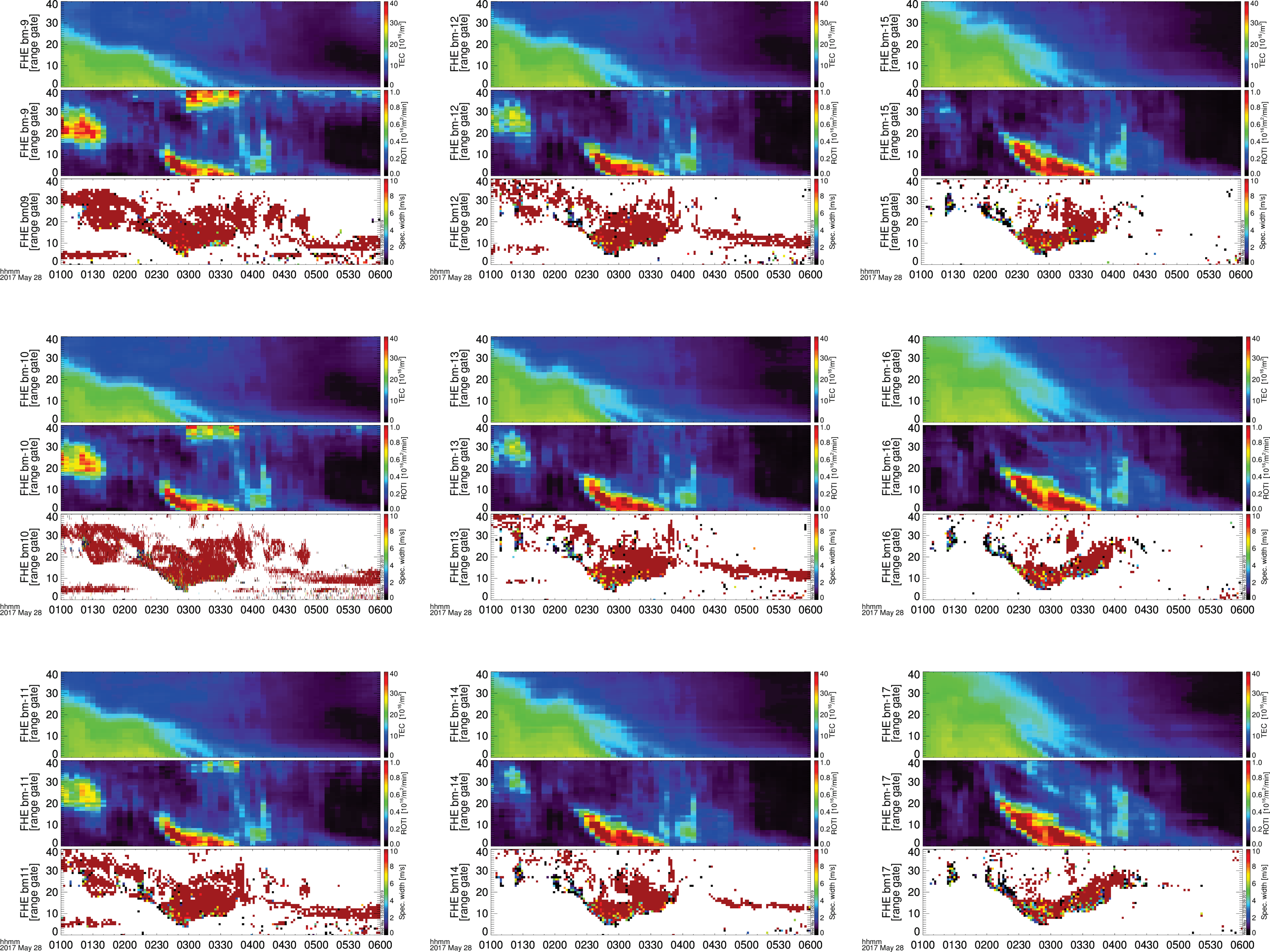
FHE bm-9 [range gate]
FHE bm09 [range gate]
FHE bm-10 [range gate]
FHE bm10 [range gate]
FHE bm-11 [range gate]
FHE bm11 [range gate]
FHE bm-12 [range gate]
FHE bm12 [range gate]
FHE bm-13 [range gate]
FHE bm13 [range gate]
FHE bm-14 [range gate]
FHE bm14 [range gate]
FHE bm-15 [range gate]
FHE bm15 [range gate]
FHE bm-16 [range gate]
FHE bm16 [range gate]
FHE bm-17 [range gate]
FHE bm17 [range gate]
TEC [10^16/m^2]
ROTI [10^16/m^2/min]
Spec. width [m/s]
hhmm
2017 May 28
0100 0130 0200 0230 0300 0330 0400 0430 0500 0530 0600

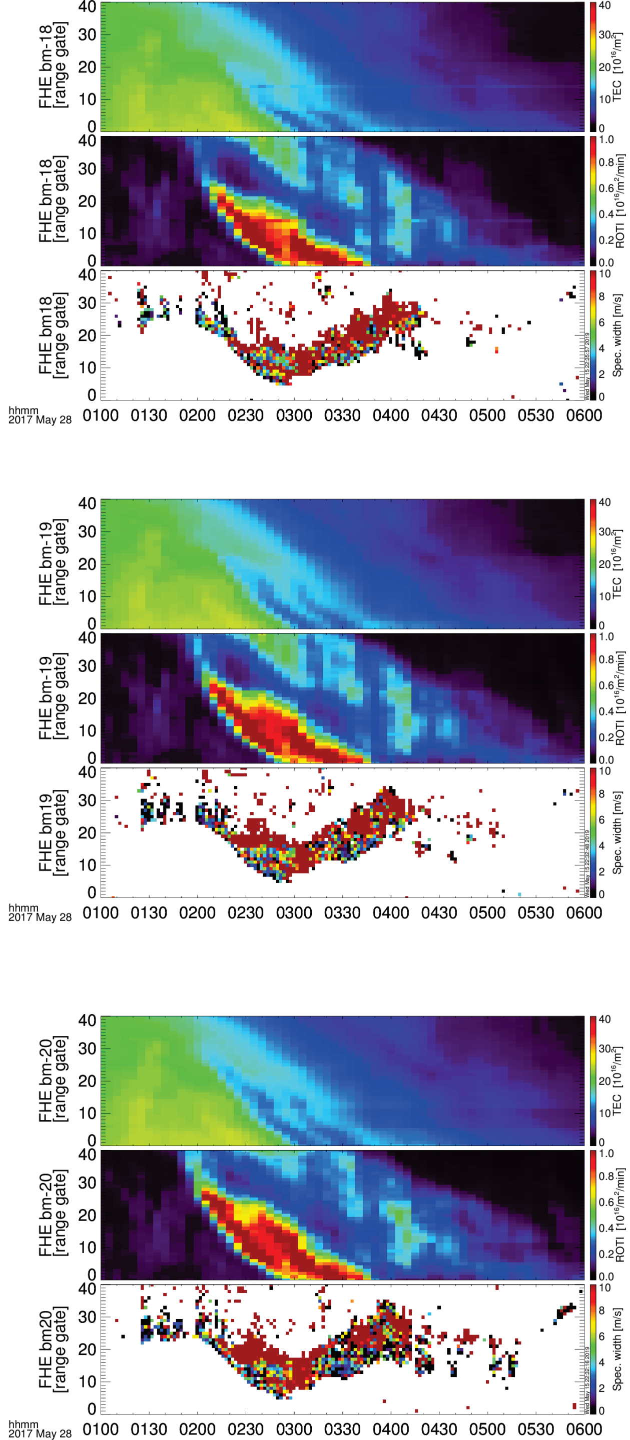

FHE bm-18 [range gate]
TEC [10^16/m^2]
ROTI [10^16/m^2/min]
FHE bm18 [range gate]
Spec. width [m/s]
FHE bm-19 [range gate]
FHE bm19 [range gate]
FHE bm-20 [range gate]
FHE bm20 [range gate]
hhmm
2017 May 28
0100 0130 0200 0230 0300 0330 0400 0430 0500 0530 0600